Indian Journal of Chemical Technology
Vol. 33, July 2026, pp. 595-608
DOI: 10.56042/ijct.v33i4.26732

Numerical investigation of magnetohydrodynamic Jeffrey fluid flow with coupled thermal and bioconvective transport

N. Golden Stepha[1] & D. Nithya[2]*
[1]Department of Mathematics, R.M.K Engineering College, Kavarapettai, Thiruvallur - 601206, Tamil Nadu, India
[2]Department of Mathematics, S.A. Engineering College, Chennai-600077, Tamil Nadu, India
*E-mail: nithyadakshna@gmail.com

Received 19 December 2025; accepted 6 July 2026

In this paper, the magnetohydrodynamic flow of a Jeffrey nanofluid over a nonlinear stretching surface by considering heat transfer, mass transfer, chemical reactions, and the motion of motile microorganisms have been analysed. The flow behaviour is influenced by magnetic forces and the presence of Hall current, which together modify the Lorentz force and affect momentum transport. Joule heating and thermal radiation are involved to represent internal heat generation and radiative effects, while Brownian motion and thermophoresis define nanoparticles movement. The concentration field is more controlled by an Arrhenius activation energy term, which captures temperature-dependent chemical reactions. The governing nonlinear partial differential equations are reduced to ordinary differential equations by using similarity transformations and solved numerically with MATLAB's bvp4c solver at a tolerance of 10^{-4}. Additionally graphical and tabular results are presented to observe how various physical parameters influence the velocity, temperature, concentration, and microorganism distributions. This study reveals that Hall current enhances momentum transport, magnetic forces suppress it, thermal radiation increases fluid temperature, and stronger convective effects promote higher microorganism accumulation near the surface.

Keywords: Activation energy, Bioconvection, Hall current, Jeffrey fluid, Magnetohydrodynamic, Slip effects

Introduction

In recent years, understanding the behaviour of fluid flow and heat transfer over stretching surfaces is vital because of their extensive industrial applications, such as polymer sheet extrusion, glass fibre drawing, metal forming, and the cooling of electronic components. An effective method to enhance thermal transport in such systems is the suspension of nanoparticles in conventional base fluids, which significantly increases their heat transfer performance. When these flows take place within porous media, the resistance offered by the porous medium introduces additional drag, thereby changing both momentum and thermal boundary layers.

The Jeffrey fluid model is quite useful among the other non-Newtonian fluid models since it takes into account both relaxation and retardation effects. This makes it a good choice for modeling viscoelastic substances like blood, paints, and polymeric liquids. Incorporating magnetohydrodynamic (MHD) effects permits control of the flow using magnetic fields, which is helpful in numerous engineering and biomedical procedures. In the presence of strong magnetic fields, Hall currents also arise, further modifying the distribution of electromagnetic forces in the fluid. Moreover, high-temperature or reactive conditions often need the consideration of additional mechanisms including thermal radiation, viscous dissipation, and chemical reactions.

The analysis of boundary layer flows over stretching surfaces has advanced greatly since the pioneering investigations of Sakiadis[1] on continuous moving surfaces and Lee[2] on thin needles, which set the framework for investigating more complex fluid behaviours. Jeffrey fluid models have subsequently gained attention for their ability to characterize viscoelastic effects more accurately than conventional Newtonian models. Early research primarily focused on the influence of magnetic fields on stretching surface flows was investigated, demonstrating the importance of magnetohydrodynamic (MHD) effects in controlling fluid motion and heat transfer characteristics[3].

Among non-Newtonian fluids, the Jeffrey fluid model has emerged as an effective constitutive model for describing the rheological behaviour of fluids possessing both relaxation and retardation characteristics. Owing to its capability to represent viscoelastic effects more realistically than Newtonian fluids, the Jeffrey model has been extensively employed in studies involving stretching surfaces and thermal transport phenomena. Ahmad and Ishak[4] analyzed MHD Jeffrey fluid flow with viscous dissipation, whereas Nadeem *et al*.[5] investigated the impact of thermal radiation on Jeffrey fluid flow over an exponentially stretching surface. The influence of homogeneous and heterogeneous chemical reactions in MHD non-Newtonian fluids was later examined by Khan *et al*.[6].

The incorporation of nanoparticles into conventional base fluids has significantly improved heat transfer performance, leading to the development of nanofluids for advanced thermal management systems. Various researchers have explored the combined influence of MHD, thermal radiation, and nanoparticle transport over stretching surfaces. Pal and Mandal[7] examined micropolar nanofluid flow with thermal radiation and non-uniform heat generation, while Hayat *et al*.[8] proposed an improved Jeffrey nanofluid model incorporating convective boundary conditions and internal heat generation. Similarly, Shehzad *et al*.[9] investigated MHD Jeffrey nanofluid flow under convective boundary conditions, and Hayat *et al*.[10] analyzed nonlinear stretching with Newtonian heating.

Entropy generation and thermal optimization have become important considerations in modern thermal engineering. In this regard, Mani and Gopi Krishna[11] investigated entropy generation in MHD Jeffrey fluid flow through an inclined channel. Mustafa *et al*.[12] presented analytical and numerical solutions for axisymmetric nanofluid flow induced by nonlinear stretching.

Further studies examined flows through porous media, where Darcy–Forchheimer drag significantly affects velocity distributions and heat transfer by Hayat *et al*.[13], while Rasool *et al*.[14] investigated Darcy–Forchheimer MHD Jeffrey nanofluid flow over stretching surfaces. The squeezing flow of Jeffrey nanofluids between parallel disks was also examined by Hayat *et al*.[15]. To handle the nonlinear and strongly coupled equations that arise in such problems, different solution strategies have been used, including the homotopy analysis method, the Keller–Box procedure, and various finite-element techniques[7,28].

To improve the accuracy of heat and mass transfer predictions, generalized transport theories based on non-Fourier heat flux and non-Fickian mass diffusion have been increasingly adopted. Khan *et al*.[16] employed generalized Fourier and Fick's laws to investigate thermal and concentration diffusion in Jeffrey nanofluids. The combined effects of constructive and destructive chemical reactions in MHD Jeffrey flow were analyzed by Hayat *et al*.[17]. Exact and numerical solutions for unsteady MHD Jeffrey fluid flow with Newtonian heating were presented by Mohd Zin *et al*.[18], while Narayana and Harish Babu[19] studied chemical reaction and thermal radiation effects on MHD Jeffrey fluid flow. Three-dimensional Jeffrey nanofluid flow subjected to nonlinear thermal radiation, Joule heating, and viscous dissipation was investigated by Ganesh Kumar *et al*.[20].

Recently, increasing attention has been devoted to bioconvection and porous media owing to their applications in biotechnology, biomedical engineering, and microscale transport systems. Ali *et al*.[21] investigated bioconvection in Jeffrey fluid flow through a Darcy–Forchheimer porous medium. Rasool *et al*.[22] analyzed entropy generation in Darcy–Forchheimer MHD nanofluid flow over nonlinear stretching surfaces. Malik[23] applied the shooting method to study MHD mixed convection flow over an inclined stretching cylinder. Ramanuja *et al*.[24] examined axisymmetric Casson nanofluid flow with slip and porous medium effects, while Mat Noor *et al*.[25] investigated squeeze flow of MHD Jeffrey fluids in porous channels with chemical reaction. Ahmad *et al*.[26] further analyzed entropy generation in Jeffrey nanofluid flow incorporating Arrhenius activation energy.

The contributions of motile microorganisms have been widely reported, showing that their activity enhances mass transfer and noticeably changes the flow characteristics[11,21,25]. Chemical reactions, nonlinear thermal radiation, and convective transport continue to receive considerable attention due to their practical significance in industrial manufacturing processes. Raju *et al*.[27] studied nonlinear thermal radiation in three-dimensional Jeffrey fluid flow with homogeneous–heterogeneous reactions. Malik *et al*.[28] investigated nonlinear stratification effects in Jeffrey fluid stagnation-point flow, whereas Mat Noor *et al*.[29] examined slip effects in squeezing Jeffrey nanofluid flow with chemical reactions. Hall and ion-slip effects in rotating Jeffrey fluids were investigated by Hari Babu *et al*.[30], while Rasheed *et al*.[31] analyzed Joule heating and viscous dissipation in MHD Jeffrey nanofluid flow over a vertically stretching cylinder. Also Khan *et al*.[32] numerically investigated MHD

Jeffrey nanofluid flow over stretching surfaces with slip effects.

Khan and Rafaqat[33] examined compressible Jeffrey fluid in peristaltic motion and reported that magnetic fields slow down the fluid while thermal radiation raises the temperature distribution. Ijaz *et al.*[34] analyzed gyrotactic ferromagnetic fluids focus to a magnetic dipole and nonlinear radiation, observing pronounced variations in both velocity and microorganism concentration. Ali *et al.*[35] studied a TiO_2–Cu/H_2O hybrid nanofluid in Jeffrey peristaltic flow with slip conditions and observed better heat transfer along with modified shear stress patterns. Agarwal *et al.*[36] examined the combined influence of micropolar and Jeffrey behaviour in the presence of MHD and radiation, identifying important alterations in velocity and temperature fields over a stretching sheet.

Mahla and Kaladhar[37] described that Hall current and magnetic fields rise entropy generation in Jeffrey fluid flow through a sloping channel, while Sowayan *et al.*[38] exhibited that fluid elasticity and radiation strongly influence heat transfer in Jeffrey nanofluid flow with variable thermal conductivity and bioconvection.

Despite these considerable efforts, only a few studies have instantaneously considered Jeffrey nanofluid flow with Hall current, melting heat transfer, activation energy, and bioconvection under Darcy–Forchheimer porous conditions. Moreover, the combined effects of chemical reactions, electromagnetic forces, and biological motility remain underexplored. The present study reports these gaps by examining steady Jeffrey nanofluid flow over a nonlinear stretching sheet, combining all these coupled effects to provide deeper insights into advanced thermal–fluid transport processes.

Problem Formulation

In this work, we investigate the flow of a Jeffrey nanofluid over a nonlinearly stretching sheet in a porous medium. The Arrhenius term describes how the reaction rate increases when the fluid temperature increases. Because of this effect, the movement of nanoparticles and the overall concentration distribution are strongly influenced by temperature changes within the boundary layer. The chemical reaction term accounts for the gain or loss of species due to reactive procedures in the fluid. When the reaction rate becomes stronger, the concentration of nanoparticles decreases more quickly, and the concentration profile becomes thinner. A uniform magnetic field B_0 is applied perpendicular to the sheet, and the Hall current effect is considered to account for the secondary flow created by the magnetic force. The velocity of the stretching surface is prescribed as $u = a_0(x+b_0)^n + L\frac{\partial u}{\partial y}$, where a_0, b_0, and n are constants representing the strength and non-linearity of the stretching, and L denotes the nonlinear velocity slip coefficient. This nonlinear slip condition accounts for micro scale effects that classical no-slip or linear slip models cannot effectively capture (Fig. 1).

Governing Equations

The governing boundary layer equations include the continuity, momentum, energy, concentration, and motile microorganism conservation equations.

Continuity Equation

$$\frac{\partial u}{\partial x} + \frac{\partial v}{\partial y} = 0 \qquad \dots (1)$$

Momentum Equation

$$u\frac{\partial u}{\partial x} + v\frac{\partial u}{\partial y} = \frac{\upsilon}{1+\lambda_s} \left[\frac{\partial^2 u}{\partial y^2} + \lambda_t\left(u\frac{\partial^3 u}{\partial x \partial y^2} + v\frac{\partial^3 u}{\partial y^3}\right)\right] - \left(\frac{\sigma B_0^2}{\rho\left(1+m^2\right)} + \frac{\upsilon\varepsilon}{k}\right)u - \frac{c_b \varepsilon}{\sqrt{k}}u^2 \qquad \dots (2)$$

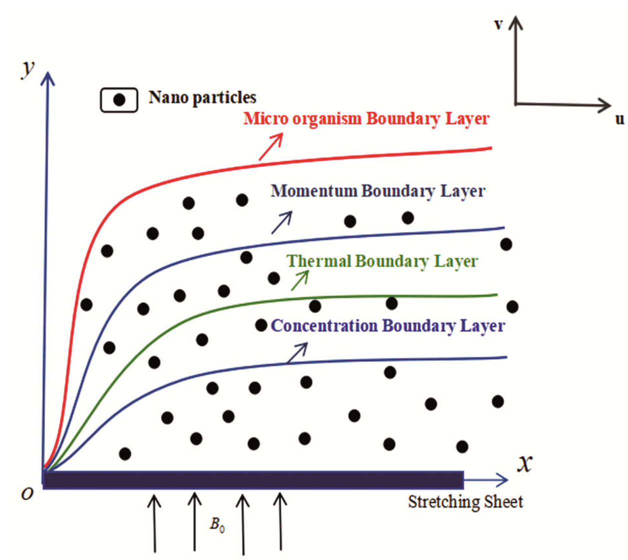

Fig. 1 — Physical model of the problem

Energy Equation

$$u\frac{\partial T}{\partial x}+v\frac{\partial T}{\partial y}=\alpha\left(\frac{\partial^2 T}{\partial y^2}\right)+\tau\left(D_B\frac{\partial C}{\partial y}\frac{\partial T}{\partial y}+\frac{D_T}{T_\infty}\left(\frac{\partial T}{\partial y}\right)^2\right)$$
$$+\frac{16\sigma^*}{3\beta\rho c_p k^*}\frac{\partial}{\partial y}\left(T^3\frac{\partial T}{\partial y}\right)+\frac{\sigma B_0^2}{\rho c_p\left(1+m^2\right)}u^2+\frac{Q_0}{\rho c_p}\left(T-T_\infty\right) \quad \ldots (3)$$

Concentration Equation

$$u\frac{\partial C}{\partial x}+v\frac{\partial C}{\partial y}=D_B\frac{\partial^2 C}{\partial y^2}+\frac{D_T}{T_\infty}\frac{\partial^2 T}{\partial y^2}-$$
$$K_n\left(C-C_\infty\right)^n\left(\frac{T}{T_\infty}\right)^m e^{-\frac{E}{kT}} \quad \ldots (4)$$

Microorganism Equation

$$u\frac{\partial N}{\partial x}+v\frac{\partial N}{\partial y}+\frac{bW_c}{C_w-C_\infty}\frac{\partial}{\partial y}\left(N\frac{\partial C}{\partial y}\right)$$
$$=D_m\frac{\partial^2 N}{\partial y^2} \quad \ldots (5)$$

The Boundary Conditions in the present problem are as given below

At the wall $y = 0$

$$u=a_0\left(x+b_0\right)^n+L\frac{\partial u}{\partial y};\ v=0;\ T=T_w;$$
$$C=C_w;\ N=N_w \quad \ldots (6)$$

In the free stream $y\to\infty$

$$u\to 0;\ T\to T_\infty;\ C\to C_\infty;\ N\to N_\infty \quad \ldots (7)$$

Non-dimensionalization

Now by introducing the following non-dimensional variables

$$\eta=\sqrt{\frac{(n+1)a_0}{2\nu}}\left(x+b_0\right)^{\frac{n-1}{2}}y;$$
$$\psi=\sqrt{\frac{2\nu a_0}{n+1}}\left(x+b_0\right)^{n+1}f(\eta),\theta(\eta)=\frac{T-T_\infty}{T_w-T_\infty}, \quad \ldots (8)$$
$$\phi(\eta)=\frac{C-C_\infty}{C_w-C_\infty},\chi(\eta)=\frac{N-N_\infty}{N_w-N_\infty}$$

The velocity components are

$$u=a_0\left(x+b_0\right)^n f'(\eta)$$
$$v=-\sqrt{\frac{(n+1)a_0\nu}{2}}\left(x+b_0\right)^{\frac{n-1}{2}} \quad \ldots (9)$$
$$\left(f+\frac{n-1}{n+1}\eta f'\right)$$

Using the above non-dimensional variables in Eqs (1)–(5), Eq. (1) becomes identically satisfied, while Eqs (2)– (5) are reduced to the following system of ordinary differential equations.

$$f^{iv}-\frac{1}{\lambda_t a_o f}$$
$$\left[\begin{array}{l} f'''+\lambda_t a_o f' f'''+\left(1+\lambda_s\right) \\ \left[ff''-f'^2-\left(M+K_p\right)f'-K_f f'^2\right]\end{array}\right]=0 \quad \ldots (10)$$

$$\left(1+\frac{4}{3}Rd\left(1+\left(\theta_w-1\right)\theta\right)^3\right)\theta''+$$
$$\Pr\left(f\theta'+\mathrm{N}b\,\theta'\phi'+Nt\theta'^2\right)+Jf'^2+Q\theta=0 \quad \ldots (11)$$

$$\phi''+Lef\phi'+\frac{Nt}{Nb}\theta''-K_r\left(1+\delta\theta\right)^m\phi^n$$
$$\exp\left(-\frac{E_1}{1+\delta\theta}\right)=0 \quad \ldots (12)$$

$$\chi''+Lbf\chi'-$$
$$Pe\left(\chi'\phi'+\left(\chi+\Omega\right)\phi''\right)=0 \quad \ldots (13)$$

based on the following boundary conditions:

$$At\ \eta=0: f(0)=0; f'(0)=1+\Lambda f''(0);$$
$$\theta(0)=1;\phi(0)=1,\chi(0)=1$$
$$In\ the\ free\ stream\ (as\ \eta\to\infty): \quad \ldots (14)$$
$$f'(\eta)\to 0;\theta(\eta)\to 0;$$
$$\phi(\eta)\to 0,\chi(\eta)\to 0$$

The dimensionless parameters that were used in Eqs (10) to (13) were defined as follows:

$$M=\frac{\sigma B_o^2}{\rho\left(1+m^2\right)a_0},\ K_p=\frac{\upsilon\varepsilon}{ka_o},K_f=\frac{C_b\varepsilon\left(x+b_o\right)}{\sqrt{k}},$$

$$Rd=\frac{16\sigma^{*}T_{\infty}^{*}}{3\beta\rho c_{p}k^{*}\upsilon},\ \Pr=\frac{\upsilon}{\alpha},\ Nb=\frac{\tau D_{B}\left(C_{w}-C_{\infty}\right)}{\upsilon},$$

$$Nt=\frac{\tau D_{T}\left(T_{w}-T_{\infty}\right)}{\upsilon T_{\infty}},\ J=\frac{\sigma B_{o}^{2}a_{o}\left(x+b_{o}\right)^{n+1}}{\rho c_{p}\left(1+m^{2}\right)\left(T_{w}-T_{\infty}\right)},$$

$$Q=\frac{Q_{o}\left(x+b_{o}\right)^{1-n}}{\rho c_{p}a_{o}},Le=\frac{\alpha}{D_{B}},$$

$$K_{r}=\frac{K_{n}\left(C_{w}-C_{\infty}\right)^{n-1}\left(x+b_{o}\right)^{1-n}}{a_{o}},\ E_{1}=\frac{E}{kT_{\infty}},$$

$$\delta=\frac{T_{w}-T_{\infty}}{T_{\infty}},Lb=\frac{\upsilon}{D_{m}},\ Pe=\frac{bW_{c}}{D_{m}},\ \Omega=\frac{N_{\infty}}{\Delta N}.$$

Dimensionless co-efficient

Skin Friction Coefficient (C_f)

$$C_{f}=\frac{\tau_{w}}{\rho u_{w}^{2}}=\sqrt{\frac{2}{(n+1)\mathrm{Re}_{x}}}\left[f''(0)+\lambda_{s}\left(\frac{3n-1}{2}f''(0)-\frac{n+1}{2}f(0)f'''(0)\right)\right] \quad \dots (15)$$

where $\mathrm{Re}_x=\frac{u_w x}{v}$ is local Reynolds number.

Nusselt Number $\left(Nu_x\right)$

$$Nu_{x}=\frac{q_{w}x}{k\left(T_{w}-T_{\infty}\right)}=-\sqrt{\frac{(n+1)\mathrm{Re}_{x}}{2}}\left[1+\frac{4}{3}R_{d}\left(1+(\theta_{w}-1)\theta(0)\right)^{3}\right]\theta'(0) \quad \dots (16)$$

Sherwood Number $\left(Sh_x\right)$

$$Sh_{x}=\frac{j_{w}x}{D_{B}\left(C_{w}-C_{\infty}\right)}=-\sqrt{\frac{(n+1)\mathrm{Re}_{x}}{2}}\phi'(0) \quad \dots (17)$$

Motile Microorganism Number $\left(Mn_x\right)$

$$Mn_{x}=\frac{q_{n}x}{D_{m}\left(N_{w}-N_{\infty}\right)}=-\sqrt{\frac{(n+1)\mathrm{Re}_{x}}{2}}\chi'(0) \quad \dots (18)$$

Numerical simulation

In this section, the Nonlinear ordinary differential equations (ODEs) Eqs (10)–(13) with the boundary constraints in Eq. (14) are typically intractable through analytical techniques. The resulting complex ODEs are transformed into the first-order ODEs by utilizing the following connections. Among the various numerical approaches reported in the literature, the bvp4c solver in MATLAB has demonstrated significant effectiveness in handling boundary value problems (BVPs), particularly those reducible to systems of first-order equations. The visual representation of the flow chart of the problem is presented in Fig. 2.

Now convert the non - linear ODE Eqs (10) to (13) to BVP problems in the following steps.

$$f=y_{1},\ f'=y_{2},\ f''=y_{3},\ f'''=y_{4};\ \theta=y_{5},$$

$$\theta'=y_{6};\ \phi=y_{7},\ \phi'=y_{8};\ \chi=y_{9},\ \chi'=y_{10}$$

$$f^{iv}=y_{4}'=\frac{1}{\lambda_{t}a_{o}y_{1}}\left[\begin{array}{c}y_{4}+\lambda_{t}a_{o}y_{2}y_{4}+\left(1+\lambda_{5}\right)\\ \left[y_{1}y_{3}-y_{2}^{2}-\left(M+K_{p}\right)y_{2}-K_{f}y_{2}^{2}\right]\end{array}\right] \quad \dots (19)$$

$$\theta''=y_{6}'=-\frac{1}{1+\frac{4}{3}R_{d}\left(1+(\theta_{w}-1)y_{5}\right)^{3}}\left[\Pr\left(y_{1}y_{6}+N_{b}y_{6}y_{8}+N_{t}y_{6}^{2}\right)Jy_{2}^{2}+Qy_{5}\right] \quad \dots (20)$$

$$\phi''=y_{8}'=K_{r}\left(1+\delta y_{5}\right)^{m}y_{7}^{n}\exp\left(-\frac{E_{1}}{1+\delta y_{5}}\right)-L_{e}y_{1}y_{8}-\frac{N_{t}}{N_{b}}y_{6}' \quad \dots (21)$$

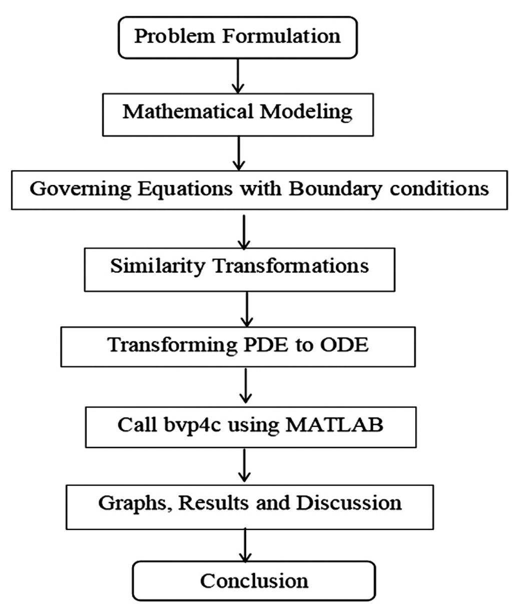

Fig. 2 — Flow chart of the problem

$$\chi'' = y_{10}' = P_e\left[y_{10}y_8 + \left(y_9+\Omega\right)y_8'\right] - L_b y_1 y_{10} \quad \ldots (22)$$

and the boundary conditions are

$$\text{when } \eta \to 0;\; y_1(a)=0,\; y_2(a)-1-\wedge y_3(a)=0,$$
$$y_5(a)-1=0,\; y_7(a)-1=0,\, y_9(a)-1=0$$
$$\text{when } \eta \to \infty;\; y_2(b)=0,\; y_5(b)=0,\; y_7(b)=0,$$
$$y_9(b)=0 \quad \ldots (23)$$

Results and Discussions

This section provides the graphical and tabulated outcomes of the Numerical simulation along with their explanation. The influence of various physical parameters on velocity, temperature, concentration and microorganism fields is analyzed and discussed in detail.

Velocity profile

The fluid velocity is influenced by the magnetic parameter M, the permeability K_p of the porous medium, and the relaxation time (λ_t) and retardation time (λ_s). Together, these factors describe how the magnetic field and the porous material affect the flow behaviour.

Fig. 3(a) depicts that the velocity distribution $f'(\eta)$ decreases when the magnetic parameter M increases. This occurs because a magnetic field creates a Lorentz force that opposes the motion of an electrically conducting fluid. As M becomes stronger, this opposing force rises, slowing down the fluid and reducing its momentum. As a result, the boundary layer becomes thicker, since the slower motion allows viscous effects to spread over a larger region. Fig. 3(b) shows that the velocity distribution $f'(\eta)$ decreases as the permeability parameter K_p increases. So, when (K_p) becomes larger, the porous medium offers more resistance to the flow, reducing the fluid's momentum and slowing it down. This slower motion weakens the velocity gradient near the surface and leads to a thicker boundary layer. Figs 3(c) and (d)

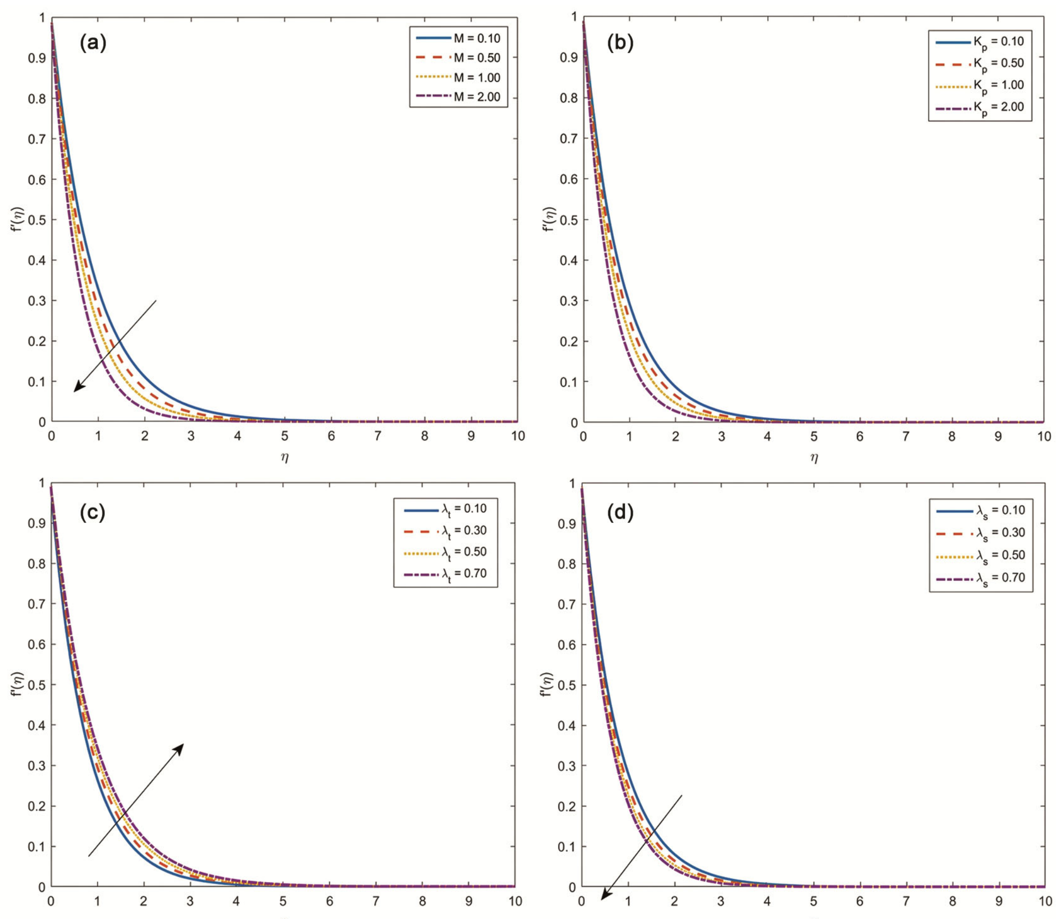

Fig. 3 — Influence of (a) M, (b) K_p, (c) λ_t and (d) λ_s on $f'(\eta)$

depict that the opposite effects of relaxation time and retardation time on the velocity distribution $f'(\eta)$. When the relaxation time increases (Fig. 5), the fluid moves faster; but when the retardation time increases (Fig. 6), the fluid becomes slower. Relaxation time indicates how long the fluid takes to return to its original shape after being stretched. A larger value allows the fluid to store elastic energy longer, helping it move more easily. In contrast, when the retardation time rises, the fluid opposes deformation more, which slows down its movement. So, a higher relaxation time supports the fluid flow faster, while a higher retardation time makes the flow slower.

Temperature Profile

Figs 4 (a)—(d) depictshow different parameters affect the temperature distribution θ(η). When the radiation parameter Rd increases (Fig. 4a), the fluid

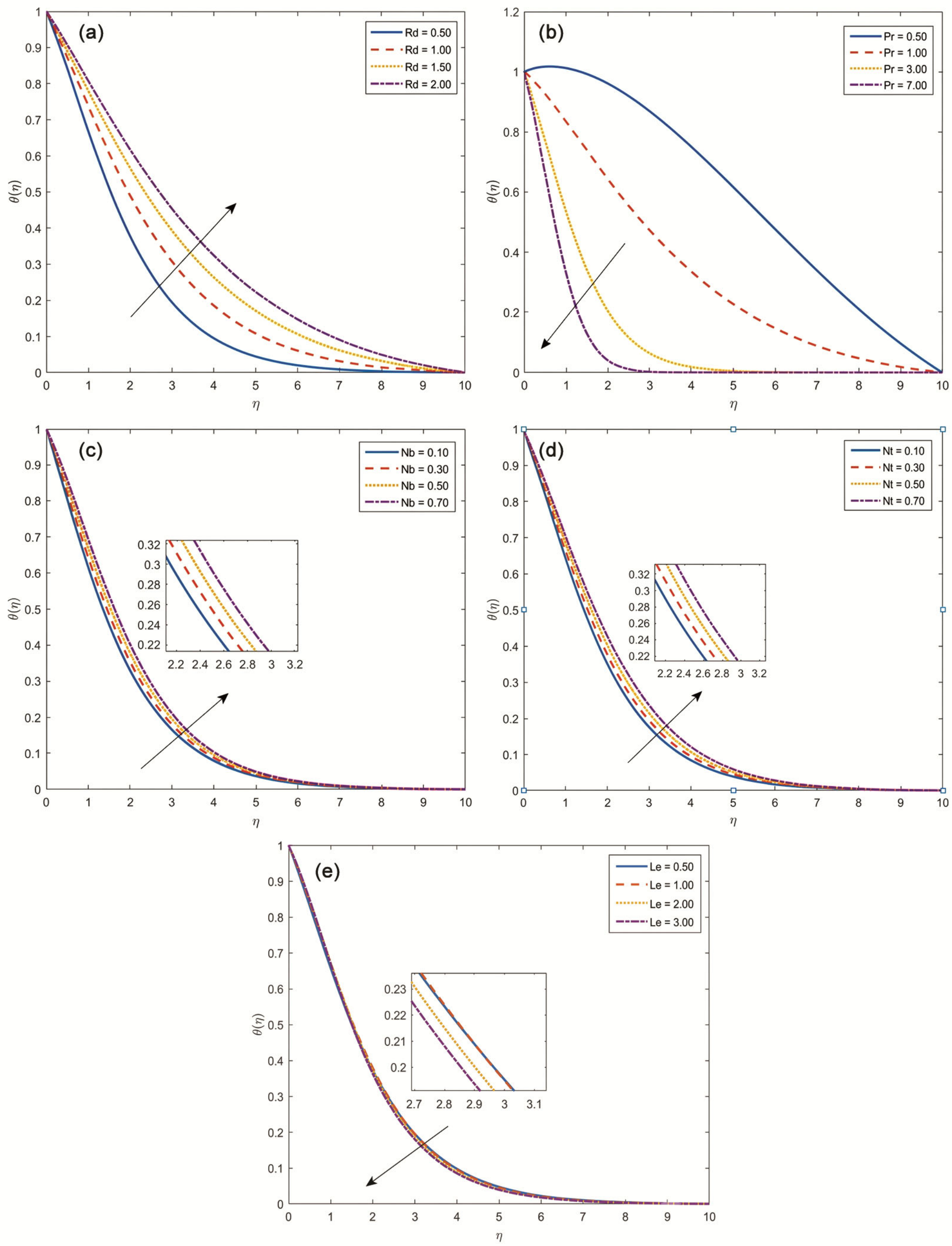

Fig. 4 — Influence of (a) *Rd*, (b) *Pr*, (c) *Nb*, (d) *Nt* and (e) *Le* on θ (η)

absorbs more heat, which raises its temperature and strengthens the thermal field. In contrast, the temperature profile θ(η). declines when the Prandtl number Pr increases (Fig. 4b), because high Pr fluids do not retain much heat inside the boundary layer, resulting in a thinner thermal layer. The temperature increases again when the Brownian motion parameter Nb rises (Fig. 4c), since stronger Brownian motion improves nanoparticle mixing and spreads heat more effectively. A similar rise in temperature distribution θ(η) is seen with higher values of thermophoresis parameter Nt (Fig. 4d), where nanoparticles move from hot to cooler regions and carry heat with them, raising the temperature within the boundary layer. Fig. 4(e) depicts that the temperature distribution θ(η) drops when the Lewis number *Le* becomes larger. A higher Le means mass diffusion dominates over heat diffusion, which reduces the amount of heat stored in the fluid. This leads to a thinner thermal boundary layer and a lower temperature throughout the flow.

Concentration profile

Fig. 5(a) depicts that increasing the Brownian motion parameter (*Nb*) decreases the concentration distribution ϕ (η) inside the boundary layer. When *Nb* becomes higher, the nanoparticles move further randomly and drift away from the wall. As fewer particles remain near the surface, the overall concentration decreases and the profile becomes flatter. Fig. 5(b depicts that the concentration distributionϕ (η) increases when the thermophoresis parameter (*Nt*) increases. With a higher *Nt*, the temperature difference pushes more particles from the hotter region towards the cooler part of the boundary layer. This enhanced movement leads to a greater build-up of particles in the cooler zone, which enhance the concentration distribution ϕ(η)

Microorganism profile

The microorganism profile χ (η) becomes lower near the wall when the Peclet number *Pe* increases as shown in Fig. 6(a). A higher Pe moves the

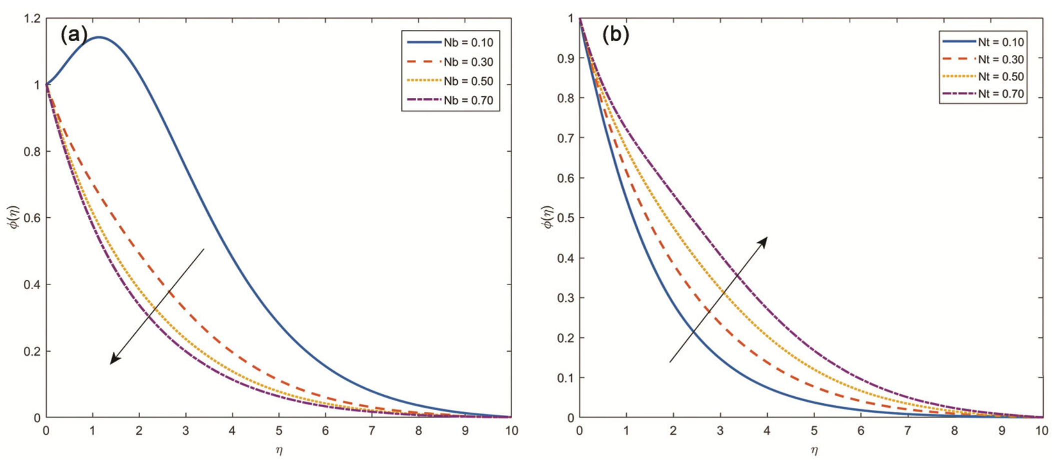

Fig. 5 — Influence of (a) Nb and (b) *Nt* on ϕ(η)

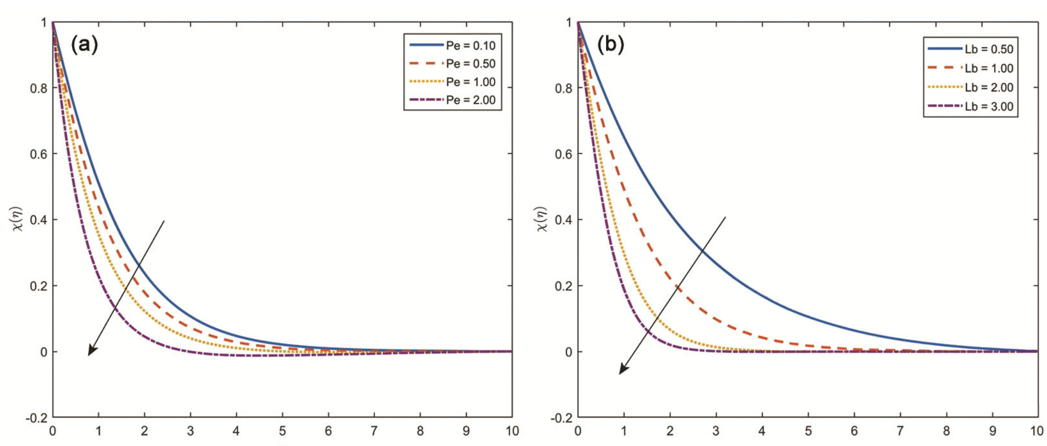

Fig. 6 — Influence of (a) *Pe* and (b) Lb on χ(η)

microorganisms forward more quickly, so they are carried away faster than they can spread back. Because of this, fewer microorganisms stay near the surface, and the boundary layer becomes thinner. Fig. 6(b) depicts that microorganism Profile χ (η) becomes lower, when the bioconvection Lewis number Lb increases. With a larger Lb, microorganisms move away from the wall more easily, so their buildup near the surface decreases. As an outcome, the concentration at the wall drops and the microorganism layer becomes thinner.

Description of Contour plot Results

The contour plots offer a comparative view of how the Nusselt number responds to different combinations of physical parameters. Each plot indicates the effects of key factors such as thermal radiation, the Prandtl number, Brownian motion, and thermophoresis. The color shading characterizes specific parameter values, making it easy to visualize how these parameters interact and how the heat transfer rate varies across the domain.

Fig. 7 shows the contour plots for the Nusselt number changes with variation of parameters together. Contour plots help to visualize the combined effects of both parameters, making it easier to understand how each one affects heat transfer. The plots demonstrates that the Nusselt number increases with higher Prandtl number Pr, as slower heat diffusion creates a steeper temperature gradient at the wall. In contrast, the Nusselt number drops when the radiation parameter Rd, Brownian motion parameter Nb, or thermophoresis parameter Nt increases, because these effects spread heat deeper into the fluid and reduce the surface temperature difference.

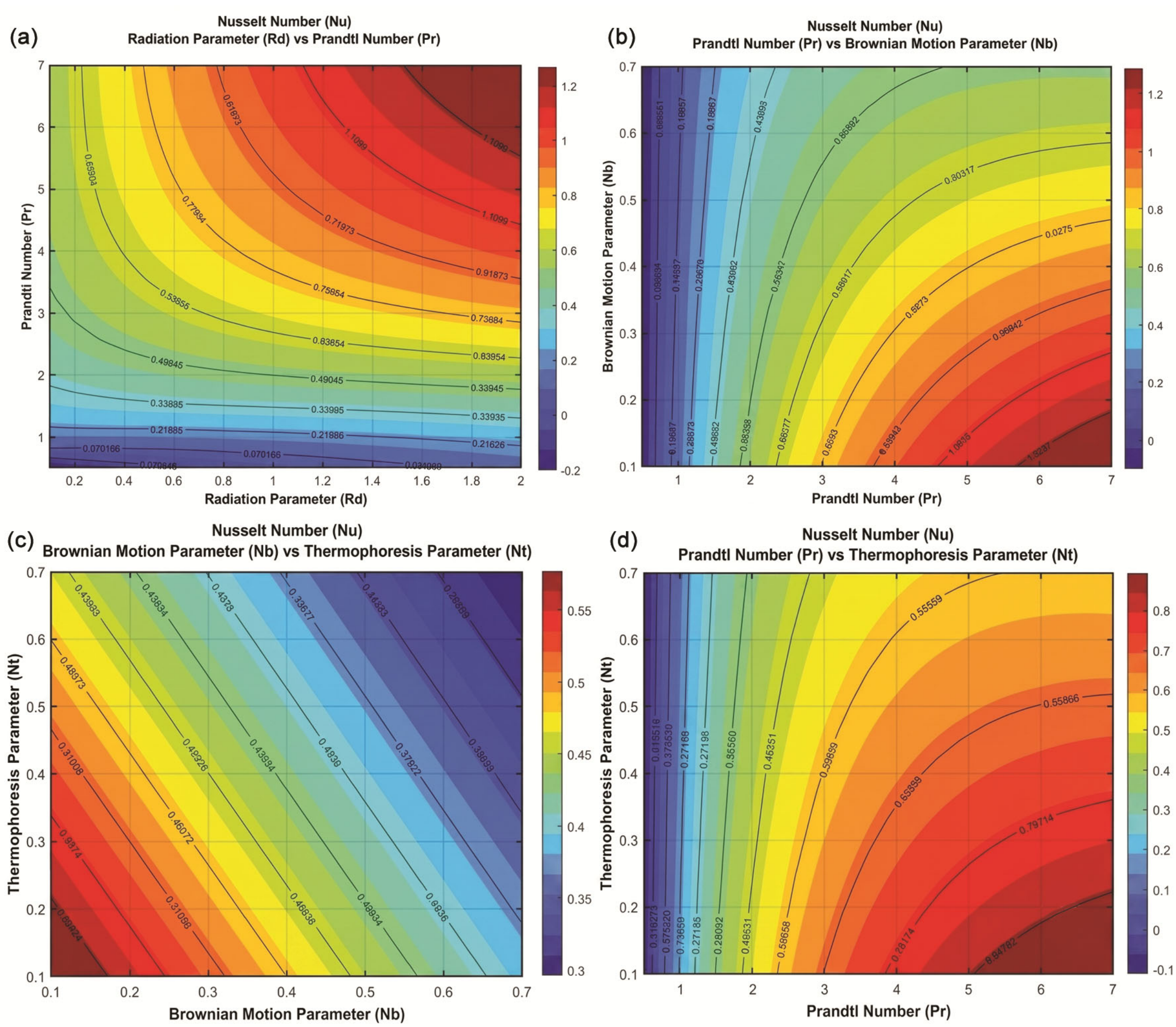

Fig. 7 — Influence of Nu_x on (a) Rd vs Pr, (b) Pr vs Nb, (c) Nb vs Nt and (d) Pr vs Nt

Streamline plots are employed to illustrate the flow pattern of a fluid. They demonstrate that the direction and relative speed of the fluid at different points, helping us understand how the fluid moves around surfaces or obstacles. Fig. 8 shows the streamlines of the flow for different values of the magnetic parameter M. When M=0.5, the streamlines are closer together near the surface, indicating faster fluid motion. As M increases to 2.5, the streamlines spread apart, displaying that the Lorentz force opposes the fluid motion and slows it down. This indicates that higher magnetic fields resist the flow, reduce momentum near the wall, and modify the flow pattern throughout the boundary layer.

Inferential statistics

Table 1 clearly displays how the main physical parameters affect the skin friction coefficient. Since the skin friction coefficient represents the flow resistance near the wall, the values in Table 1 help elucidate how this resistance changes.

Effect of various parameters on Nusselt Number

Table 2 demonstrates the influence of selected dimensionless parameters on the Nusselt number, which represents the dimensionless heat transfer rate at the surface. The Nusselt number is particularly exaggerated by the radiation parameter (Rd), Prandtl number (Pr), Brownian motion parameter (Nb), and thermophoresis parameter (Nt).

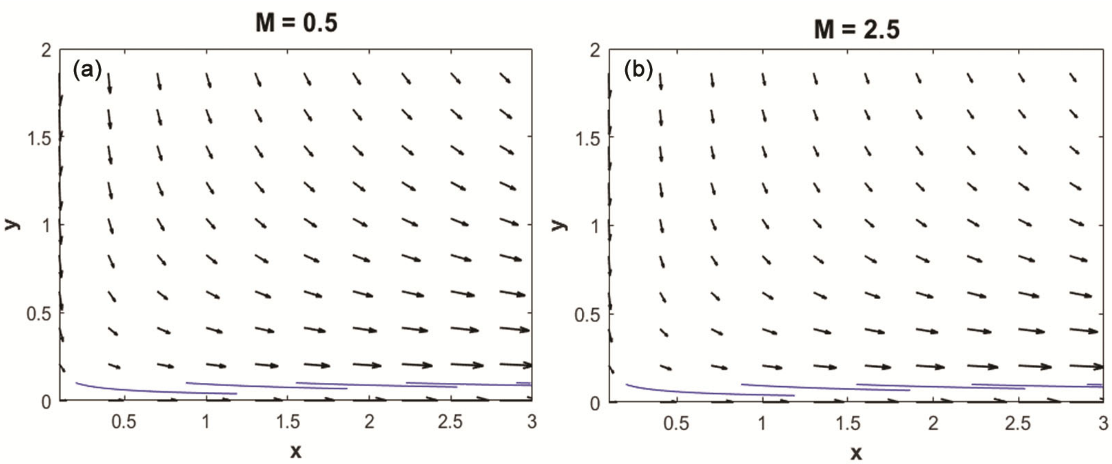

Fig. 8 — Stream lines for magnetic parameters (a) M = 0.5 and (b) M = 2.5

Table 1 — Effect of various parameters on skin friction coefficient

M	K_p	K_f	λ_t	λ_s	Skin friction (C_f)	Effects	Reason
0.1					-1.1992	$M\uparrow\Rightarrow C_f\downarrow$	The Lorentz force due to a magnetic field act as a resistive force opposing the flow.
0.5					-1.3627		
1					-1.542		
2					-1.847		
	0.1				-1.3466	$K_p\uparrow\Rightarrow C_f\downarrow$	Higher permeability implies a more porous medium, offering less resistance to fluid flow.
	0.5				-1.5001		
	1				-1.6722		
	2				-1.9716		
		0.1			-1.3866	$K_f\uparrow\Rightarrow C_f\downarrow$	The Forchheimer term accounts for inertial resistance in the porous medium; as K_f increases, flow resistance decreases.
		0.3			-1.435		
		0.5			-1.482		
		0.7			-1.5277		
			0.1		-1.3047	$\lambda_t\uparrow\Rightarrow C_f\uparrow$	Increasing relaxation time allows the fluid to retain elastic energy longer, which raises the velocity profile.
			0.3		-1.4183		
			0.5		-1.5238		
			0.7		-1.6227		
				0.1	-1.3627	$\lambda_s\uparrow\Rightarrow C_f\downarrow$	Increasing retardation time makes the fluid resist deformation more, slowing its response and reducing the velocity.
				0.3	-1.2516		
				0.5	-1.1636		
				0.7	-1.0916		

Table 2 — Effect of various parameters on Nusselt Number

Rd	*Pr*	*Nb*	*Nt*	Nu_x	Effects	Reason
0.5				0.40909	$Rd\uparrow \Rightarrow Nu_x\uparrow$	Thermal radiation enhances energy transport in the fluid, increasing the temperature gradient at the wall and thus heat transfer.
1				0.44694		
1.5				0.47553		
2				0.50479		
	0.5			-0.09675	$\Pr\uparrow \Rightarrow Nu_x\downarrow$	When Pr increases, the thermal boundary layer becomes thinner because heat transfers more slowly. This means the temperature gradient is steeper, and the overall temperature within the fluid is typically lower.
	1			0.17163		
	3			0.58784		
	7			0.7866		
		0.1		0.54023	$Nb\uparrow \Rightarrow Nu_x\uparrow$	Brownian motion increases nanoparticle dispersion, which tends to thicken the thermal boundary layer, increase the heat transfer rate.
		0.3		0.47171		
		0.5		0.40909		
		0.7		0.35217		
			0.1	0.44618	$Nt\uparrow \Rightarrow Nu_x\uparrow$	When the *Nt* increases, the temperature profile typically increases as well, and the thickness of the thermal boundary layer alsoincreases. This is because a higher *Nt* value enhances the driving forces of temperature and concentration gradients, leading to faster heat and mass transfer rates.
			0.3	0.40909		
			0.5	0.37456		
			0.7	0.34239		

Table 3 — Effect of various parameters on Shear wood Number

Nb	*Nt*	*Le*	Sh_x	Effects	Reason
0.1			-0.069617	$Nb\uparrow \Rightarrow Sh_x\downarrow$	Enhances nanoparticle diffusion, decreasing concentration gradients and mass transfer.
0.3			0.39415		
0.5			0.4848		
0.7			0.52221		
	0.1		0.53724	$Nt\uparrow \Rightarrow Sh_x\uparrow$	When the thermophoresis parameter *Nt* increases, the concentration profile generally increases due to the enhanced thermophoretic force, which drives particles away from the hot surface and into the fluid domain.
	0.3		0.4848		
	0.5		0.44603		
	0.7		0.41936		
		0.5	0.28298	$Le\uparrow \Rightarrow Sh_x\downarrow$	Increasing Lewis number → lower mass diffusivity → slower diffusion of species → thinner concentration boundary layer → lower concentration profile.
		1	0.4848		
		2	0.81512		
		3	1.0756		

Table 4 — Effect of various parameters on Motile microorganism

Lb	*Pe*	Mn_x	Effects	Reason
0.5		0.4062	$Lb\uparrow \Rightarrow Mn_x\downarrow$	As the bioconvection Lewis number increases, the diffusion of microorganisms becomes less effective, leading to reduced spreading and a decrease in the microorganism profile.
1		0.61194		
2		0.92879		
3		1.1771		
	0.1	0.36053	$Pe\uparrow \Rightarrow Mn_x\downarrow$	As the Peclet number increases, the boundary layer becomes thinner and the microorganism profile decreases because of limited spreading.
	0.5	0.54476		
	1	0.78021		
	2	1.2643		

Effect of various parameters on Shear wood Number

Table 3 displays the influence of key dimensionless parameters on the Sherwood number (Sh_x), which quantifies the mass transfer rate at the surface. The Sherwood number is strongly influenced by nanoparticle dynamics and species diffusivity, particularly through parameters such as Brownian motion (Nb), thermophoresis (Nt), and the Lewis number (Le).

Effect of various parameters on motile microorganism

Table 4 illustrates how variations in the bioconvection Lewis number (Lb) and the Peclet number (Pe) change the density of motile microorganisms (Mn_x), suggesting how strongly microorganisms accumulate or separate near the surface.

Comparative analysis

Comparative analyses with the reported literature are shown in Tables 5-7.

Table 5 — Comparative analysis of Nusselt number (Nu_x) and skin friction (C_f)

Parameter	Pr	Naresh Kumar *et al.*[39]	Present study
Nusselt number (Nu_x)	0.7	1.300	1.337
	2.0	1.591	1.588
	7.0	4.750	4.799
Skin friction (C_f)	0.7	0.443	0.467
	2.0	0.455	0.482
	7.0	0.460	0.491

Table 6 — Comparative Analysis with Hayat *et al.* [17]

Pr	Hayat *et al.*	Present study
0.7	0.8102	0.8101
2.0	1.5935	1.5882
7.0	3.2889	3.2885

Table 7 — Comparison of $-\theta'(0)$ $for\ M = \beta = \phi = 0$ (baseline validation)

Pr	Ishak[3]	Pal[7]	Present study
0.7	0.8086	0.808631	0.8024
2.0	1.5919	1.591876	1.5882
7.0	3.2907	3.290654	3.2899

Conclusion

In this study we analyzed the complex interaction of magnetohydrodynamic and bioconvection effects in a Jeffrey fluid flow over a nonlinear stretching surface by including key physical mechanisms with Hall current, velocity slip, thermal radiation, chemical kinetics along with activation energy, and the motility of microorganisms. The governing equations, transformed via similarity variables, are numerically solved using MATLAB's bvp4c solver revealing several prominent trends:

- Increasing the value of magnetic parameter (M), it decreases the velocity distribution, conversely higher values of permeability of the porous medium (K_p), the velocity distribution increases.
- Thermal radiation (Rd) enhances extra energy to the boundary layer, which increases the fluid temperature and promotes stronger thermal diffusion.
- A higher values Prandtl number (Pr) indicates lower thermal diffusivity, since heat spreads more slowly, the temperature in the fluid decreases.
- Increasing the value of Brownian motion parameter Nb exhibits a decrease in the temperature profile on the other hand it increases the concentration profile.
- Increasing the value of thermophoresis parameter Nt, it displays an increase of temperature and concentration profiles.
- As Lb increases, the enhanced diffusion spreads the microorganisms over a wider region, limiting their build-up and resulting in a smoother overall distribution.
- A rise in the Peclet number (Pe) strengthens convective transport relative to diffusion. As a result, microorganisms tend to accumulate nearer to the wall.

Conflict of Interest

The authors declare no conflict of interest.

Nomenclature

u,v	Velocity component
x, y	Cartesian co-ordinates
λ_s	Ratio of relaxation time to the retardation time
λ_t	Retardation time
B_0	Magnitude of applied magnetic field / viscosity parameter
C_b	Forchheimer coefficient
D_B	Brownian diffusion coefficient
D_T	Thermophoretic diffusion coefficient
D_m	Diffusivity of microorganism
m	Hall current
υ	Kinematic viscosity
W_c	Constant maximum cell swimming speed
E	Activation energy
σ^*	Electrical conductivity
ρ	Fluid density / liquid density
T	Temperature of the liquid
T	Ambient fluid temperature
C	Concentration of nano particle
C_∞	Ambient fluid concentration
N	Rescaled density of motile microorganism
N_∞	Ambient fluid microorganism
c	Stretching constant
T_W	Wall temperature
C_W	Wall concentration
M	Magnetic field
K_p	porosity parameter
K_f	Forchheimer term
Rd	Non-linear radiation
Pr	Prandtl number
Nb	Brownian motion parameter
Nt	Thermophoresis parameter
J	Joule heating
Q	Heat absorption parameter
Le	lewis number
K_r	chemical reaction parameter
E_1	dimensionless activation energy
δ	temperature difference ratio

Lb Lewis number for microorganism
Pe Peclet number
Ω Microorganism concentration ratio

References

1 Sakiadis B C, Boundary-layer behaviour on continuous solid surfaces: I. Boundary-layer equations for two-dimensional and axisymmetric flow, *AIChE J*, 7 (1961) 26.
2 Lee L L, Boundary layer over a thin needle, *Phys Fluids*, 10 (1967) 820.
3 Ishak A, Nazar R & Pop I, Hydromagnetic flow and heat transfer adjacent to a stretching vertical sheet, *Heat Mass Transf*, 44 (2008) 921.
4 Ahmad K & Ishak A, MHD flow and heat transfer of a Jeffrey fluid over a stretching sheet with viscous dissipation. *Malays J Math Sci*, 10 (2016) 311.
5 Nadeem S, Zaheer S & Fang T, Effects of thermal radiation on the boundary layer flow of a Jeffrey fluid over an exponentially stretching surface, *Numer Algorithms*, 57 (2011) 187.
6 Khan I, Malik M Y, Salahuddin T & Abbas Z, Homogenous-heterogeneous reactions in MHD flow of Powell-Eyring fluid over a stretching sheet with Newtonian heating, *Neural Comput Appl*, 30 (2018) 3581.
7 Pal D & Mandal G, Thermal radiation and MHD effects on boundary layer flow of micropolar nanofluid past a stretching sheet with non-uniform heat source/sink, *Int J Mech Sci*, 126 (2017) 308.
8 Hayat T, Aziz A, Muhammad T & Alsaedi A, A revised model for Jeffrey nanofluid subject to convective condition and heat generation/absorption, *PLoS One,* 12 (2017) e0172518.
9 Shehzad S A, Hayat T & Alsaedi A, MHD flow of Jeffrey nanofluid with convective boundary conditions, *J Braz Soc Mech Sci Eng*, 37 (2015) 873.
10 Hayat T, Bashir G, Waqas M & Alsaedi A, MHD flow of Jeffrey liquid due to a nonlinear radially stretched sheet in presence of Newtonian heating. *Results Phys*, 6 (2016) 817.
11 Mani R & Krishna G G, Entropy analysis of MHD flow of Jeffrey fluid in an inclined channel, *Heat Transf*, 51 (2022) 5789.
12 Mustafa M, Khan J A, Hayat T & Alsaedi A, Analytical and numerical solutions for axisymmetric flow of nanofluid due to non-linearly stretching sheet, *Int J Non-Linear Mech*, 71 (2015) 22.
13 Hayat T, Shah F, Hussain Z & Alsaedi A, Darcy-forchheimer flow of Jeffrey nanofluid with heat generation/absorption and melting heat transfer, *Therm Sci*, 23 (2019) 3833.
14 Rasool G, Shafiq A & Durur H, Darcy-forchheimer relation in magnetohydrodynamic Jeffrey nanofluid flow over a stretching surface, *Discrete Contin Dyn Syst Ser S*, 14 (2021) 2531.
15 Hayat T, Abbas T, Ayub M, Muhammad T & Alsaedi A, On squeezed flow of Jeffrey nanofluid between two parallel disks, *Appl Sci*, 6 (2016) 346.
16 Khan M, Shahid A, Malik M Y & Salahuddin T, Thermal and concentration diffusion in Jeffery nanofluid flow over an inclined stretching sheet: A generalized Fourier's and Fick's perspective, *J Mol Liq*, 251 (2018) 7.
17 Hayat T, Waqas M, Khan M I & Alsaedi A, Impacts of constructive and destructive chemical reactions in magnetohydrodynamic (MHD) flow of Jeffrey liquid due to nonlinear radially stretched surface, *J Mol Liq*, 225 (2017) 302.
18 Mohd Z N A, Khan I & Shafie S, Exact and numerical solutions for unsteady heat and mass transfer problem of Jeffrey fluid with MHD and Newtonian heating effects, *Neural Comput Appl*, 30 (2018) 3491.
19 Narayana P V S & Babu D H, Numerical study of MHD heat and mass transfer of a Jeffrey fluid over a stretching sheet with chemical reaction and thermal radiation, *J Taiwan Inst Chem Eng*, 59 (2016) 18.
20 Kumar K G, Rudraswamy N G, Gireesha B J & Krishnamurthy M R, Influence of nonlinear thermal radiation and viscous dissipation on three-dimensional flow of Jeffrey nanofluid over a stretching sheet in the presence of Joule heating, *Nonlin Eng*, 6 (2017) 207.
21 Ali M H, Abbas S T, Sohail M & Singh A, Study of bioconvection phenomenon in Jefferey model in a Darcy-Forchheimer porous medium, *Bio-Nano Sci*, 14 (2024) 4666.
22 Rasool G, Shafiq A, Khan I, Baleanu D, Nisar K S & Shahzadi G, Entropy generation and consequences of MHD in Darcy-Forchheimer nanofluid flow bounded by non-linearly stretching surface, *Symmetry*, 12 (2020) 652.
23 Malik M Y, Application of shooting method on MHD thermally stratified mixed convection flow of non-Newtonian fluid over an inclined stretching cylinder, *J Phys: Conf Ser*, 822 (2017) 012007.
24 Ramanuja M, Raju B T, Nagaradhika V, Madhusudhana R B, Durgaprasad P & Raju C S K, Significance of axisymmetric flow of Casson Darcy unsteady slip flow in a suspension of nanoparticles with contracting walls, *J Nanofluids*, 11 (2022) 350.
25 Noor N A M, Shafie S & Admon M A, Impacts of chemical reaction on squeeze flow of MHD Jeffrey fluid in horizontal porous channel with slip condition, *Physica Scripta*, 96 (2021) 035216.
26 Ahmad S, Khan M I, Hayat T, Waqas M & Alsaedi A, Irreversibility in two-dimensional magneto-nanomaterial flow of Jeffrey fluid with Arrhenius activation energy, *Int J Numer Meth Heat Fluid Flow*, 29 (2019) 4485.
27 Raju C S K, Sandeep N & Gnaneswara R M, Effect of nonlinear thermal radiation on three-dimensional Jeffrey fluid flow in the presence of homogeneous-heterogeneous reactions, *Int J Eng Res*, 21 (2016) 52.
28 Malik H T, Farooq M & Ahmad S, Significance of nonlinear stratification in convective Falkner-Skan flow of Jeffrey fluid near the stagnation point, *Int Commun Heat Mass Transf*, 120 (2021) 105032.
29 Noor N A M, Shafie S & Admon M A, Slip effects on MHD squeezing flow of Jeffrey nanofluid in a horizontal channel with chemical reaction, *Mathematics*, 9 (2021) 1215.
30 Babu B H, Srinivasa R P & Varma S V K, Hall and ion-slip effects on MHD free convection flow of rotating Jeffrey fluid over an infinite vertical porous surface, *Heat Transf*, 50 (2021) 1776.
31 Ur-Rasheed H, Al-Zubaidi A, Islam S, Saleem S, Khan Z & Khan W, Effects of Joule heating and viscous dissipation on magnetohydrodynamic boundary layer flow of Jeffrey nanofluid over a vertically stretching cylinder, *Coatings*, 11 (2021) 353.
32 Khan M, Imran M, Khan M R, Beinane S A O & Alzahrani A, Numerical analysis of heat transfer and flow characteristics of

Jeffrey nanofluid over stretched surfaces with MHD and slip effects, *Math Methods Appl Sci*, 48 (2025) 8641.
33 Khan A A & Rafaqat R, Effects of radiation and MHD on compressible Jeffrey fluid with peristalsis, *J Therm Anal Calorim*, 143 (2021) 1971.
34 Ijaz M, Nadeem S, Ayub M & Mansoor S, Simulation of magnetic dipole on gyrotactic ferromagnetic fluid flow with nonlinear thermal radiation, *J Therm Anal Calorim*, *143*(2021) 2053.
35 Ali A, Saleem S, Mumraiz S, Saleem A, Awais M & Marwat D N K, Investigation on TiO_2–Cu/H_2O hybrid nanofluid with slip conditions in MHD peristaltic flow of Jeffrey material, *J Therm Anal Calorim*, 143 (2021) 1985.
36 Agarwal V, Singh B & Nisar K S, Numerical analysis of heat transfer in magnetohydrodynamic micropolar Jeffrey fluid flow through porous medium over a stretching sheet with thermal radiation, *J Therm Anal Calorim*, 147 (2022) 9829.
37 Mahla R & Kaladhar K, Irreversibility analysis of Jeffrey fluid flow in a sloping channel with Hall current, thermal radiation, and inclined magnetic field effects, *J Therm Anal Calorim*, 149 (2024) 7705.
38 Sowayan A S, Majeed A, Khan S U & Riaz A, Thermally radiative bioconvective flow of Jeffrey nanofluid with variable thermal conductivity: PST and PHF analysis, *J Thermal Anal Calorim*, 150 (2025) 4681.
39 Kumar N, Srinivasu G, Setty B S & Ramanuja M, MHD Darcy-Forchheimer flow of Jeffrey nanofluid over a stretching sheet considering melting heat transfer and viscous dissipation, *CFD Lett*, 16 (2024) 131.